ACS APPLIED ENGINEERING MATERIALS

pubs.acs.org/acsaenm

Article

Multiscale Process Modeling of Semicrystalline PEEK for Tailored Thermomechanical Properties

Khatereh Kashmari, Hashim Al Mahmud, Sagar U. Patil, William A. Pisani, Prathamesh Deshpande, Marianna Maiaru, and Gregory M. Odegard*

Cite This: ACS Appl. Eng. Mater. 2023, 1, 3167−3177

Read Online

ACCESS | Metrics & More | Article Recommendations | Supporting Information

ABSTRACT: Polyether ether ketone (PEEK) is a semicrystalline thermoplastic that is used in high-performance composites for a wide range of applications. Because the crystalline phase has a higher mass density than that of the amorphous phase, the evolution of the crystalline phase during high-temperature annealing processing steps results in the formation of residual stresses and laminate deformations, which can adversely affect the composite laminate performance. Multiscale process modeling, utilizing molecular dynamics, micromechanics, and phenomenological PEEK crystal kinetic laws, is used to predict the evolution of volumetric shrinkage, elastic properties, and thermal properties, as a function of crystalline phase evolution, and thus annealing time, in the 306−328 °C temperature range. The results indicate that lower annealing temperatures in this range result in a faster evolution of thermomechanical properties and shrinkage toward the pure crystalline values. Therefore, from the perspective of composite processing, it may be more advantageous to choose the higher annealing rates in this range to slow the volumetric shrinkage and allow PEEK stress relaxation mechanisms more time to relax internal residual stresses in PEEK composite laminates and structures.

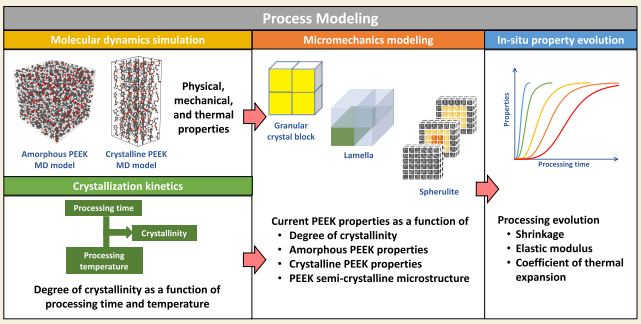

KEYWORDS: *molecular dynamics, micromechanics, materials genome initiative, integrated computational materials engineering, crystallization kinetics*

1. INTRODUCTION

Polyether ether ketone (PEEK) is a high-performance semicrystalline thermoplastic polymer of considerable commercial interest in the aerospace industry due to its exceptional mechanical properties and high-temperature resistance. It is often used as the matrix in composite materials for structural components subjected to significant thermal and mechanical loads.

The crystalline/amorphous-phase topology of PEEK spans multiple length scales[1−4] and is known to evolve kinetically when annealed at elevated temperatures.[5,6] The transformation of the higher energy amorphous phase to the lower energy crystalline phase is known to be accompanied by volumetric shrinkage. This shrinkage has the potential to cause residual stresses during composite processing because of the presence of a network of stiffer reinforcing inclusions,[7] similar to the evolution of residual stresses in thermoset composites due to chemical crosslinking shrinkage.[8,9] Excessive residual stresses adversely affect the composite performance and can result in shape deformations in the final composite component.[1,7−15]

Process modeling can be used to optimize the manufacturing parameters of composite materials to obtain optimal physical, mechanical, and thermal properties.[1,16−21] Such processing parameters include temperature, hold times, and cooling rates. Optimization of these parameters can reduce the magnitude of the internal residual stresses resulting from the crystallization shrinkage as well as the residual stresses that result from the differential thermal contractions between fiber, crystalline PEEK, and amorphous PEEK phases during the cooling cycle at the end of processing. Although process modeling can be used to optimize the process parameters to mitigate these residual stresses, a comprehensive understanding of the evolution of PEEK properties during the processing/crystallization process is required as inputs. The characterization of PEEK properties and crystalline nano/micro-topology is difficult and expensive to achieve through experimental approaches. Thus, computational methods are a more favorable means of obtaining the evolution of properties during processing.[22−24]

Pisani et al.[3] used molecular dynamics (MD) modeling and the multiscale generalized method of cells (MSGMC)[4] to

Received: September 26, 2023
Revised: October 18, 2023
Accepted: October 18, 2023
Published: November 2, 2023

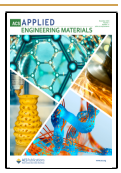

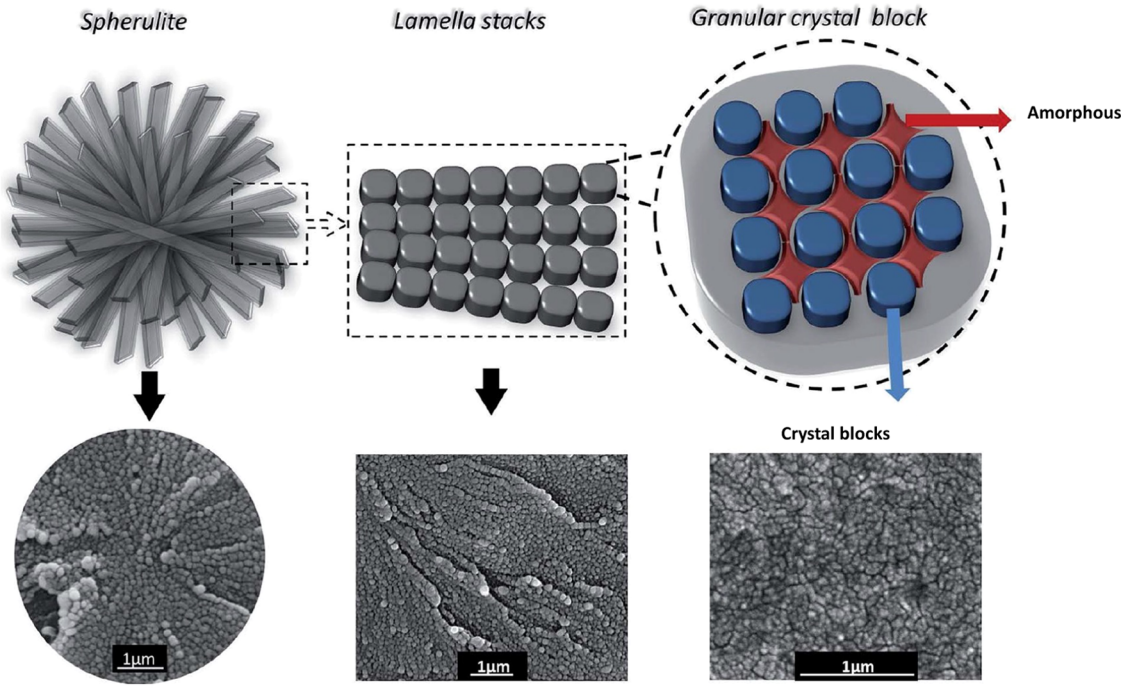

Figure 1. Microstructure of semicrystalline polymers. Reproduced from ref 4 with permission from the Royal Society of Chemistry.

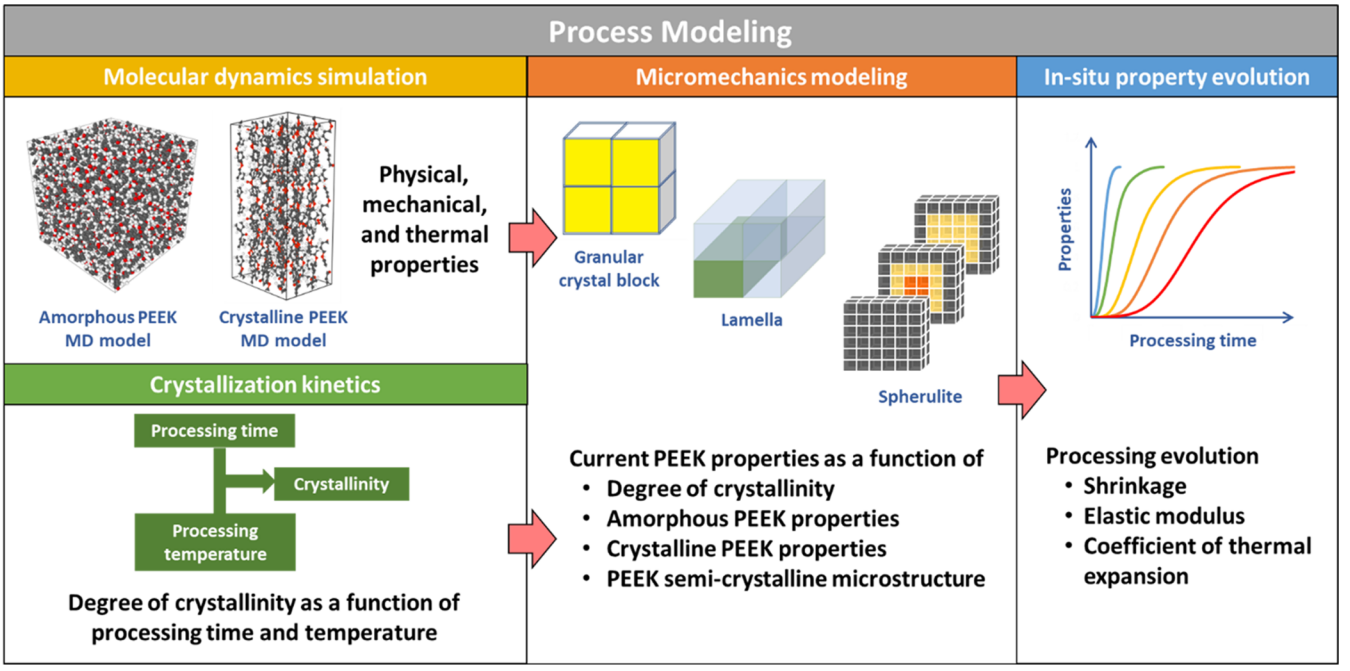

Figure 2. Multiscale modeling workflow for semicrystalline PEEK.

predict the mechanical properties of semicrystalline PEEK. MD modeling was used to predict the properties of the individual crystalline and amorphous phases. The MSGMC method utilized those properties as input and was used to predict the bulk-level mechanical properties based on crystalline topology, and the resulting predictions agreed well with experimental data. Despite the excellent contribution of the work of Pisani et al., a computational multiscale study has not yet been performed on PEEK that relates the molecular structure to the temporal evolution of mechanical properties during processing. Such a relationship is critical for the accurate process modeling of PEEK composites.

In this study, the thermomechanical properties of PEEK have been predicted as a function of processing conditions using multiscale modeling and crystallization kinetics. The combined MD and MSGMC approach of Pisani et al.[3] has been expanded to include a more comprehensive MD PEEK crystalline model (27 times larger) for better statistical sampling and crystallization kinetics[25] to accurately and efficiently establish the thermomechanical properties of semicrystalline PEEK during processing. This information is

https://doi.org/10.1021/acsaenm.3c00586
ACS Appl. Eng. Mater. 2023, 1, 3167−3177

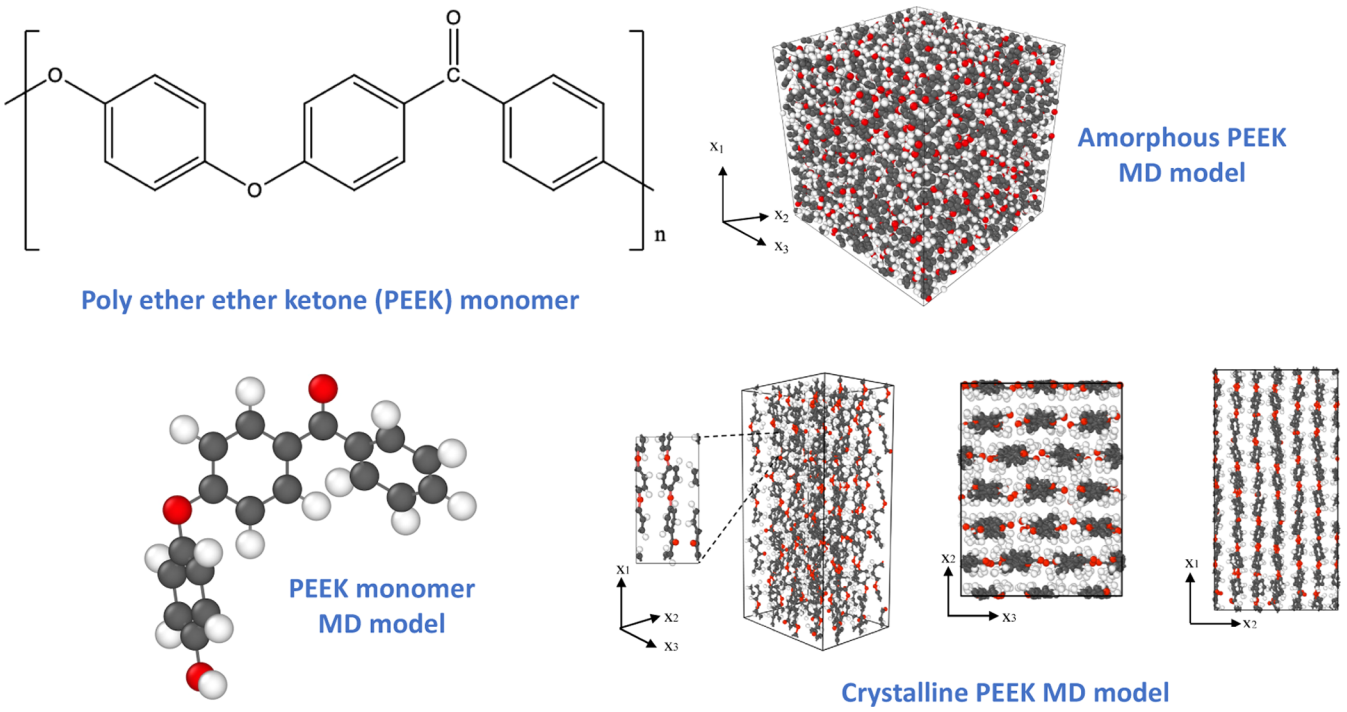

Figure 3. PEEK molecular structure and MD models of amorphous and crystalline PEEK.

critical for accurate process modeling and optimization of processing parameters for PEEK composites with minimal residual stresses.

2. PEEK MOLECULAR AND MICROSTRUCTURE

For temperatures under the equilibrium melting temperature, the PEEK crystalline phase is thermodynamically more stable than the amorphous phase; thus, there is a strong thermodynamic driving force for crystal growth in PEEK.[26] When the crystalline phase is nucleated, the crystals grow in a three-dimensional radial pattern (spherulites), and the spherulites continue to grow until they make physical contact with other spherulites. The resulting material morphology consists of three characteristic microstructures: spherulites, lamellae, and granular crystal blocks (Figure 1).[4] Because of the complex morphology of the growing crystalline phase, complete crystallization cannot occur, resulting in the coexistence of crystalline and amorphous regions at the metastable state.[4,27] The growth rate of spherulites is directly affected by the temperature.[5,6] Spherulites (Figure 1, left) are composed of lamellae (Figure 1, center) with a thickness between 100 and 800 nm depending on the temperature of crystallization. Due to the radial pattern and the higher mass density of the crystalline phase, the core region of spherulites is denser than the outer regions. The lamellae are composed of granular crystal blocks (GCB) (Figure 1, right), which are composed of crystalline and amorphous regions.[4,6]

3. MULTISCALE MODELING PROCEDURES

The multiscale modeling workflow used herein is shown in Figure 2. MD simulation was used to model the molecular structure, physical properties, mechanical properties, and thermal properties of the amorphous and crystalline regions of PEEK. Micromechanical modeling was used to model the microstructure of the semicrystalline material and predict bulk-level properties. Process modeling was used to predict the shrinkage and properties of the semicrystalline PEEK as a function of the processing conditions. Details of each of these three modeling steps are included in this section.

The reactive interface force field (IFF-R),[28−35] a modification of the interface force field,[28] was applied to describe the interactions between the atoms in the polymer system. The open-source large-scale atomic/molecular massively parallel simulator (LAMMPS) MD simulation software package was used for all MD simulations in this study. Nose−Hoover algorithms were used for both the thermostat and barostat for all simulations discussed herein.[36,37]

3.1. Amorphous Phase Modeling

The MD modeling algorithm for the amorphous phase consisted of three stages: model building, polymerization, and property prediction. Five different amorphous PEEK molecular replicates were constructed for statistical sampling. A single PEEK monomer (Figure 3, upper left) was simulated by using the NVT (constant volume and temperature) ensemble over 100 ps to obtain a relaxed conformation (Figure 3, lower left). The relaxed monomer was replicated eight times in each direction of a 150 × 150 × 150 $Å^3$ simulation box, resulting in 512 monomers and 18,432 atoms with a gas-phase mass density of 0.06 g/cm^3.

The gas-phase MD models were slowly densified to obtain the bulk mass density of the polymer. The densification process was performed at 27 °C over 10 ns to gradually change the volume of the simulation box in 15 stages to achieve an initial target mass density of 1.30 g/cm^3[28] After reaching the target density, the models were annealed using the NVT ensemble by ramping up the polymer system temperature to 327 °C, immediately followed by a ramp down with the rate of 25 °C/ns to room temperature. The annealing process was followed by an equilibration simulation at room temperature in the NPT (constant pressure and temperature) ensemble, followed by a molecular structure minimization using the conjugate gradient algorithm (Polak−Ribiere) to fully relax the

https://doi.org/10.1021/acsaenm.3c00586
ACS Appl. Eng. Mater. 2023, 1, 3167−3177

molecules. The minimizations utilized an energy tolerance of 10^{-4} (unitless), a force tolerance of 10^{-6} (kcal/mol·Å), 100 maximum iterations, and 1000 maximum force/energy evaluations.[38] Figure 3 (top right) shows a representative fully densified model. Spatial density profiles were generated and were relatively smooth, which indicates that the monomers were uniformly distributed in each direction.

After densification, polymerization was simulated over 5 ns at 27 °C with 1 fs time steps. Figure S1 in the Supporting Information (SI) shows the polymerization process of the PEEK monomers. The polymerization reactions were simulated by creating chemical bonds between O atoms and C atoms in the phenyl rings of the adjacent molecule using the "fix bond/react" command in LAMMPS.[39] There are two criteria involved in the bond formation with this command. First, the minimum and maximum distances between the two reactive atoms to initiate a reaction were defined, and second, the probability of bond formation was assigned.[39] The polymerization was performed in three steps. First, the minimum reaction distance, maximum reaction distance, and probability were set to 0.0, 4.0, and 0.00001, respectively, until 50% of all C−O reactive groups were bonded (henceforth referred to as the extent of the reaction). Second, the maximum reaction distance and the probability were changed to 5.0 Å and 0.0001, respectively, until an extent of reaction of 85% was achieved. Finally, the maximum reaction distance and probability were set to 6.0 Å and 0.9, respectively, until a maximum and steady value of extent of reaction was achieved. The final average extent of the reaction of all five models was 90.8%. Once the polymerization was completed, the free hydrogen molecules were deleted from the simulation box.

Annealing simulations were performed on all five polymerized PEEK models. The simulation temperature was ramped down from 327 to 27 °C over 12 ns with a cooling rate of 25 °C/ns to relieve the residual stresses resulting from the polymerization. Finally, all models were subjected to equilibration simulation using the NPT ensemble at 27 °C and 1 atm pressure over 1.5 ns. The final average mass density of all five models was 1.254 ± 0.002 g/cm^3, which is in good agreement with the experimental value reported by Blundell and Osborn, 1.262 g/cm^3.[40]

3.2. Amorphous-Phase Mechanical Properties

The five polymerized replicates of amorphous PEEK were subjected to mechanical shearing simulations in the x_3-x_2, x_3-x_1, and x_2-x_1 planes at room temperature (27 °C) and various PEEK processing temperatures from 306 to 328 °C. The "fix deform" command in LAMMPS was utilized to apply a strain rate of 2×10^8 s^{-1} over 500 ps with 0.1 fs time steps, leading to 18% engineering shear strain. The average of all three shear moduli (G) over the five replicates for both temperatures was determined (Table 1). A representative shear stress−strain curve is shown in Figure S2, and the shear modulus was the slope of the shear stress−shear strain curve below the bilinear breakpoint.

The MD models of amorphous PEEK were also subjected to bulk modulus deformation simulations at room temperature. The simulation boxes were subjected to two separate pressures (1 and 5000 atm) over 1 ns using the NPT ensemble. The difference in the volume at the two pressures (ΔV) was determined to predict the bulk modulus (K).[41] The SI provides a detailed justification for determining the elastic properties via shear and bulk simulations, based on previous simulation work[42] and our own simulations.

Table 1. Mechanical Properties of Amorphous PEEK Using IFF-R at Room Temperature[a]

properties	27 °C using IFF-R	ReaxFF[3]	experiment
mass density (g/cm^3)	1.254 ± 0.002	1.30 ± 0.01	1.26[40,43]
E (GPa)	2.87 ± 0.40	2.90 ± 0.40	2.78[2,44]
G (GPa)	1.01 ± 0.15	1.02 ± 0.15	0.97[2,44]
K (GPa)	6.19 ± 0.13		
ν	0.42 ± 0.01	0.42 ± 0.01	
σ_y (MPa)	85.30 ± 11.0		

[a]MD results from Pisani et al.[3] using the ReaxFF force field are included, with other experimental results from the literature.

Polymetric materials are yielded mostly due to deviatoric stresses; thus, the von Mises stress criterion was used to quantify the equivalent stress of the multiaxial stress states in the shear simulations for determining the uniaxial yield strength. The material was assumed to yield at the breakpoint of the shear stress−strain plots (e.g., see Figure S2), and the yield strength (σ_y) was the corresponding von Mises stress at the break point. The average yield strength values for the replicate systems at both temperatures are provided in Table 1.

In addition to the mechanical properties determined using the IFF-R force field, Table 1 also includes values from Pisani et al.[3] utilizing the reactive force field (ReaxFF)[45] at room temperature and other literature sources.[2,3,43,44] The comparison of the predicted properties with IFF-R and ReaxFF properties at room temperature shows excellent agreement. When the properties predicted herein using IFF-R are compared with the experimental values from the literature, it is important to note that there are no empirical mechanical properties of purely amorphous PEEK available. Some studies have tried to address the mechanical properties of purely amorphous PEEK using a combination of experimental and statistical methods,[2,46] which match well with the MD results.

3.3. Amorphous-Phase Thermal Properties

The molecular dynamics protocol used in this study for predicting the glass transition temperature (T_g) of PEEK is based on a large body of work by the authors,[30,32,41,47−49] including a recent comprehensive study on the T_g prediction of polymers.[29] The general approach for predicting T_g is to use a simulated heating ramp through the glass transition region. The glass transition phenomenon is a result of the changes that occur in the chain interactions, free volume levels, and van der Waals forces at a critical temperature, that is unique to each amorphous material. Odegard et al. have provided a comprehensive explanation of the T_g phenomenon elsewhere.[29] It is important to note that temperature fluctuations naturally occur during the heating ramp (as is physically expected in a nanometer-sized system), which is typical for all MD simulations, even in constant-temperature ensembles.

To predict the T_g of the amorphous phase of PEEK, all five fully polymerized models were heated to 327 °C with a heating rate of 25 °C/ns in the NPT ensemble under 1 atm pressure. A representative plot of the mass density over the entire range of temperature is shown in Figure S3. The figure shows the expected volumetric response of the system subjected to a heating cycle, including the statistically and physically necessary temperature fluctuations.[29,41] It is also apparent in the figure that the fluctuations increase with increasing temperatures, which is expected, given the increases in thermal

https://doi.org/10.1021/acsaenm.3c00586
ACS Appl. Eng. Mater. 2023, 1, 3167−3177

energy at higher temperatures and the corresponding thermostat process. It is important to note that the well-known cooling rate effect in polymers affects measured and predicted T_g values,[50] that is, higher cooling rates correspond to higher apparent T_g values. However, this study specifically uses heating cycles for T_g prediction to avoid the cooling rate effect.[29,50]

A bilinear regression was fitted to the mass density vs temperature plot, and the break point was taken to be the T_g.[29,48] The predicted T_g value is provided in Table 2. It is important to note that the literature value[43] provided in Table 2 is slightly higher than the predicted value because it was measured on PEEK with 30−35% crystallinity content, which increases the T_g.[51]

Table 2. Thermal Properties of Amorphous PEEK

properties	MD prediction	experiment[43,52]
T_g (°C)	128.67 ± 23.03	142
CTE above T_g ($\times 10^{-5}$ °C^{-1})	13.13 ± 1.56	16.30
CTE below T_g ($\times 10^{-5}$ °C^{-1})	6.07 ± 0.51	6.40

The coefficient of linear thermal expansion (CTE) was calculated based on the results from the T_g simulations, above and below T_g. The simulation box volumes were plotted vs temperature for the heating cycles (Figure S4), and linear regression lines were fit to the curves above and below T_g.[27] The predicted CTE values are provided in Table 2 along with experimental values from the literature.[52]

3.4. Crystalline Phase Modeling

The PEEK crystal unit cell is orthorhombic (space group *Pbcn*) containing two molecules with the lattice constants of a = 6.80 Å, b = 6.00 Å, and c = 14.28 Å.[53] PEEK crystal supercells were constructed by replicating the unit cell three times along each axis, resulting in 27 monomers and 1836 atoms, as shown in Figure 3 (lower right). Five samples of the crystalline PEEK supercell were generated for statistical sampling. The MD models were equilibrated in the NVT ensemble at 27 °C over 3 ns, followed by NPT simulations at 27 °C for 12 ns. The resulting mass density of the crystalline models was 1.40 ± 0.001 g/cm^3, which is in good agreement with the experimental value of 1.40 g/cm^3 reported by Blundell et al.[40] The equilibrated MD models had the supercell parameters a = 17.90 ± 0.08 Å, b = 22.81 ± 0.22 Å, and c = 44.88 ± 0.03 Å.

3.5. Crystalline-Phase Properties

The five replicate models were subjected to uniaxial tensile deformations along the x_1, x_2, and x_3 directions at a strain rate of 2×10^8 s^{-1} applied over 1 ns to predict the elastic modulus in each direction. The NPT ensemble and the Nose−Hoover barostat were used to allow Poisson contractions in the transverse directions. The simulation boxes were transformed to triclinic boxes to predict the shear modulus, and shear simulations were performed with respect to the x_1−x_2, x_1−x_3, and x_1−x_2 planes at a strain rate of 2×10^8 s^{-1} applied over 500 ps (for 18% engineering shear strain). The time step was set to 0.1 fs for all simulations. Representative tensile stress−strain data along the x_2-axis for crystalline PEEK at 300 K are shown in Figure S5. The corresponding Young's modulus, shear modulus, Poisson's ratio, and yield strength values are reported in Table 3.

Table 3. Mechanical Properties of Crystalline PEEK

properties	27 °C using IFF-R	ReaxFF[3]
E_1 (GPa)	142.14 ± 7.40	117.14 ± 5.48
E_2 (GPa)	4.75 ± 0.23	8.51 ± 1.11
E_3 (GPa)	7.30 ± 0.62	8.37 ± 1.02
G_{12} (GPa)	0.94 ± 0.22	0.89 ± 0.27
G_{13} (GPa)	1.42 ± 0.13	1.40 ± 0.74
G_{23} (GPa)	2.33 ± 0.36	1.52 ± 0.90
ν_{12}	1.37 ± 0.11	0.69 ± 0.07
ν_{13}	−0.43 ± 0.04	1.92 ± 0.93
ν_{23}	0.32 ± 0.04	0.50 ± 0.08
σ_{y1} (MPa)	9655.22 ± 0.48	
σ_{y2} (MPa)	222.02 ± 0.05	
σ_{y3} (MPa)	280.37 ± 0.05	

The CTE values of crystalline PEEK were determined by heating each replicate from −173 to 327 °C with 25 °C/ns heating rate. The resulting volume vs temperature graph was used to evaluate CTE values predicted in each direction. The CTE predictions are shown in Table 4.

Table 4. Thermal Properties of Crystalline PEEK

properties	MD predictions	experiment[52]
CTE along x_1 ($\times 10^{-5}$ °C^{-1})	−0.73 ± 0.22	−1.40
CTE along x_2 ($\times 10^{-5}$ °C^{-1})	14.45 ± 1.59	12.00
CTE along x_3 ($\times 10^{-5}$ °C^{-1})	4.29 ± 0.79	5.00

3.6. Volumetric Shrinkage

To calculate the volumetric shrinkage of semicrystalline PEEK at the bulk level, the volume of amorphous and crystalline PEEK was predicted at each processing temperature. The total volume as a function of crystallinity content was obtained at each processing temperature using the rule of mixtures

$$V_t = f_{cr} V_{cr} + (1 - f_{cr}) V_a$$

where V_t is the total volume of the semicrystalline PEEK, f_{cr} is the crystallinity fraction, and V_a and V_{cr} are the volume of the amorphous and crystalline PEEK, respectively. The volumetric shrinkage percentage was determined using

$$S(\%) = \frac{(V_a - V_t)}{V_a} \times 100$$

which corresponds to the change in the volume as a function of crystallinity.

3.7. Viscous Response Correction

Before using the molecular level predicted properties as input for the microscale modeling (details below), the raw MD-predicted properties needed to be mapped to the corresponding laboratory-scale values to account for the viscoelastic effects associated with the strain rate and temperature. The mapping is required because of the short time scales associated with the MD simulation. In this work, a phenomenological method proposed by Patil et al.[54] was implemented to map the elastic properties of amorphous PEEK predicted from MD (E_{MD}) to the corresponding laboratory-scale values (E).

The mapping of the Young's modulus was established using[54]

$$\frac{E}{E_{MD}} = f_\alpha(\alpha) f_\tau(\tau)$$

https://doi.org/10.1021/acsaenm.3c00586
ACS Appl. Eng. Mater. 2023, 1, 3167−3177

where

$$\alpha \equiv \frac{\dot{\varepsilon}}{\dot{\varepsilon}_{MD}}, \quad \tau \equiv 1 - \frac{T}{T_r}$$

$\dot{\varepsilon}_{MD}$ is the strain rate associated with MD time scales; $\dot{\varepsilon}$ is the experimental strain rate; T_r is the reference temperature, which should be the highest temperature for which experimental Young's modulus data are available; T and T_r are expressed in degrees Kelvin, while α and τ are dimensionless scalars that are valued between 0 and 1; f_α (α) is a phenomenological factor associated with the strain rate, and f_τ (τ) is a phenomenological factor associated with temperature. The factors can be expressed using

$$f_\alpha(\alpha) = \alpha_a \ln(\alpha) + \alpha_b$$

$$f_\tau(\tau) = \{1 - [1 + e^{(\tau - \tau_0/\tau_\sigma)}]^{-1}\}\{1 - [1 + e^{(\tau - \tau_*{}^a/\tau_*{}^b)}]^{-1}\}$$

There are six phenomenological parameters associated with these equations (α_a, α_b, τ_0, τ_s, $\tau_*{}^a$, $\tau_*{}^b$). Experimental strain rate data[55,56] were used to determine α_a and α_b, and experimental tensile test data at varying temperatures[43] were used to predict τ_0, τ_s, $\tau_0{}^*$, and $\tau_b{}^*$, as described in detail elsewhere.[54] Table 5 shows the predicted viscoelastic dimensionless mapping factors for PEEK.

Table 5. Viscoelastic Dimensionless Mapping Factors Associated with the Mechanical Properties Predicted with MD

material	α_a	α_b	τ_0	τ_σ	$\tau_*{}^a$	$\tau_*{}^b$
PEEK	0.0277	1.624	0.11	0.006	0.16	0.07

3.8. Micromechanics Modeling

Once the elastic properties of the amorphous and crystalline phases were evaluated using MD simulations, they were input into micromechanics models to predict the bulk thermomechanical properties of the semicrystalline PEEK (Figure 2, center). The MSGMC method[3] was utilized to model the PEEK semicrystalline microstructures, including GCBs, lamella, and spherulites. A repeating unit cell (RUC) was employed to represent the periodic material microstructure at each length scale. Each RUC was discretized into subcells, which represent a specific characteristic microstructure. The MD properties were used for the amorphous and crystalline phases of the GCBs and the amorphous phase of the lamella. The GCB contains 86.2% crystalline volume fraction and 13.8% amorphous phase based on the reported value in the literature.[4] The corresponding lamella RUC contains three subcells of amorphous PEEK and one subcell of GCB.

The aspect ratio of the GCB phase of the lamella could be changed to control the overall crystallinity content of the lamella structure. The spherulite was generated from lamella structures with varying degrees of crystallinity. The crystalline volume fractions corresponded to the crystalline concentrations in different regions of the spherulite, which increased from the outer region to the center of the spherulite. The details of these varying concentrations are provided by Pisani et al.[3] It was assumed that the bulk semicrystalline properties were those of the spherulite phase. Similar to Pisani et al.,[3] this assumption was made based on the typical topology of semicrystalline PEEK, in which most of the bulk is composed of portions of the spherulite phase.[4,6] Thus, for simplicity, it was assumed that the overall spherulite crystallinity corresponded to the bulk crystallinity.

MSGMC was also used for the prediction of the CTE of semicrystalline PEEK. The CTE values of the amorphous and crystalline phases (Tables 2 and4, respectively) were used as input for the GCB and lamella, and the process followed the same approach as that with the elastic properties. MAC/GMC utilizes Levin's theorem to obtain the CTE of multiphase materials.[57] The results from the modeling discussed in this section are described in detail in Section 4. Complete details on the RUCs have been reported by Pisani et al.[3]

3.9. Process Modeling

With the dependence of mechanical and thermal properties of a semicrystalline PEEK material on the relative crystallinity content established in the previous modeling steps, the next step was to predict the properties as a function of processing time and temperature (Figure 2, right). The processing temperature and cooling rate of a thermoplastic highly influence the degree of crystallinity.[58] Specifically for PEEK, cooling rates of 10−600 °C/min obtain a degree of crystallinity between 25 and 30% and cooling rates of more than 700 °C/min lead to a completely amorphous PEEK microstructure since the spherulite topology has insufficient time to form.[59,60] Motz et al.[61,62] performed an experimental study on the PEEK crystallization process and observed that the onset and completion of crystallization depend on the cooling rate and processing temperature.[48] Therefore, an accurate understanding of crystallization kinetics is required to link the processing conditions to semicrystalline mechanical and thermal properties.

PEEK crystallization has two stages. The primary stage is characterized by heterogeneous nucleation by inclusions or nucleating agents inside the polymer melt. The secondary stage occurs with homogeneous growth of the spherulites and is governed by the processing temperature.[63,64] The relative crystallinity, $X(t)$, can be described by the Avrami equation

$$X(t) = 1 - e^{(-Kt^n)} \quad (1)$$

where K is the crystallinity ratio constant, n is the Avrami exponent, and t is the processing time. The Avrami exponent is material-dependent, and the crystallinity ratio constant, K, is proportional to the temperature at the given pressure, which can be modeled using the Arrhenius equation[65,66]

$$K = Ae^{(-(E/R(T_m - T))} \quad (2)$$

where E and A are the activation energy and pre-exponential factor, respectively, and $T_m - T$ is the surfusion function with the melting temperature of 343 °C.

As discussed above, isothermal PEEK crystallization is a dual-mechanism process, thus ideally requiring two different Avrami exponents.[66−68] Velisaris and Seferis[67] recommended applying the parallel Avrami model for PEEK to model the primary and secondary crystallization processes together. This approach includes a weighting factor for both primary and secondary processes, dependent on the temperature and cooling rate. Ko et al.[69] included a secondary mechanism onset time into the parallel Avrami model for PEEK to simulate the delayed onset of secondary crystallization. Bessard et al.[66] observed that the weighting factor of the primary crystallization reduces as the crystallization temperature increases and thus concluded that as the temperature increases

https://doi.org/10.1021/acsaenm.3c00586
ACS Appl. Eng. Mater. 2023, 1, 3167−3177

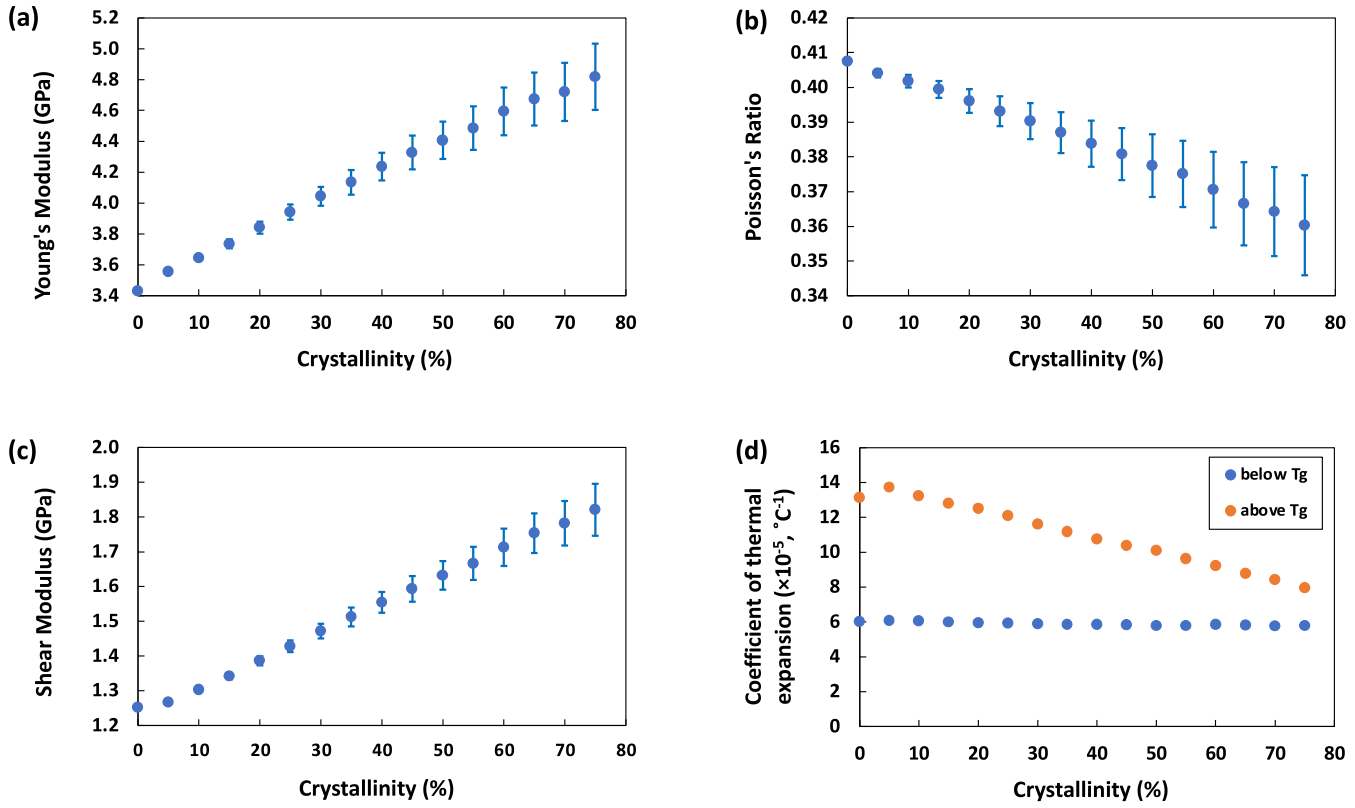

Figure 4. (a) Young's modulus, (b) Poisson's ratio, (c) shear modulus, and (d) coefficient of thermal expansion of semicrystalline PEEK as a function of the crystallinity content. The errors bars for (d) are smaller than the symbols.

during isothermal crystallization, the contribution of secondary crystallization increases.[66]

Seo et al.[25] developed a crystallization model based on the dual crystallization mechanism suggested by Velisaris and Seferis.[67] This model utilizes two competing crystal growth processes, and the relative crystallinity is given by

$$X(t) = \frac{1 - e^{(-(t/t_c))^{n_p}}}{1 - e^{(-(t/t_c))^{n_p}} + e^{\left(-t_c^{-n_p} t^{n_s} (-\ln(0.5)/t_c^{-n_p})^{(1-(n_p/n_s))}\right)}} \quad (3)$$

where t is the processing time; n_s and n_p are the Avrami constants for secondary and primary crystallization processes, respectively; and t_c is the time required to obtain a relative crystallinity of 63%. Equation 3 is derived from an alternative form of the Avrami equation

$$X(t) = 1 - e^{(t/t_c)^n} \quad (4)$$

Comparison between eqs 1 and 4 reveals that $K = t_c^{-n}$. Further details on the derivation of eq 3 are provided elsewhere.[25] The parameters used in this study are listed in Table S1. The relative crystallinity of PEEK over time in the range of 306−328 °C is presented in Figure S6.

4. RESULTS AND DISCUSSION

Figure 4 presents the bulk thermal and mechanical properties of semicrystalline PEEK as functions of crystallinity obtained using the results in Tables 1−4. Figure 4a,4c shows that the moduli increase with increases in crystallinity, which is expected because of the stiffer nature of the crystalline phase. Figure 4b shows that Poisson's ratio steadily decreases with increasing crystallinity. Figure 4d shows that the CTE below T_g is not affected by the crystallinity content, while the CTE above T_g decreases as crystallinity increases. Due to the reduced mobility of the molecular structure below T_g, an increase in crystallinity has a lesser impact on thermal expansion compared to that above T_g.

In order to derive the uncertainties of properties at the continuum level based on uncertainties at the atomic level, the MD properties listed in Tables 1−4 were randomly sampled from a uniform distribution of their corresponding standard deviation range during each multiscale micromechanics run (as explained in the previous section). For instance, when considering the amorphous Young's modulus, a value within the range of 2.26−3.34 GPa (equivalent to 2.87 ± 0.4 GPa from Table 1) was randomly chosen for each run. Finally, the mechanical properties of the spherulite were determined by taking the average of the results obtained from 300 distinct runs. From Figure 4, it is evident that the standard deviation of the mechanical properties increases with increasing levels of crystallinity. This is likely due to the relatively large uncertainty in the E_1 of the crystalline phase (7.4 GPa, Table 3) compared to the amorphous isotopic value (0.4 GPa, Table 1). Thus, for higher crystallinity levels, the higher uncertainty associated with the crystalline phase will have a larger impact on the uncertainty of the bulk semicrystalline modulus.

Figure 5a shows the predicted volumetric shrinkage during the processing of semicrystalline PEEK due to crystallization for a range of processing temperatures. Using the relation between the crystallization content and volumetric shrinkage and eq 6, the volumetric shrinkage was predicted as a function of processing time for different processing temperatures. The data indicate that the lower processing temperatures in this range drive faster volumetric shrinkage, which is directly

https://doi.org/10.1021/acsaenm.3c00586
ACS Appl. Eng. Mater. 2023, 1, 3167−3177

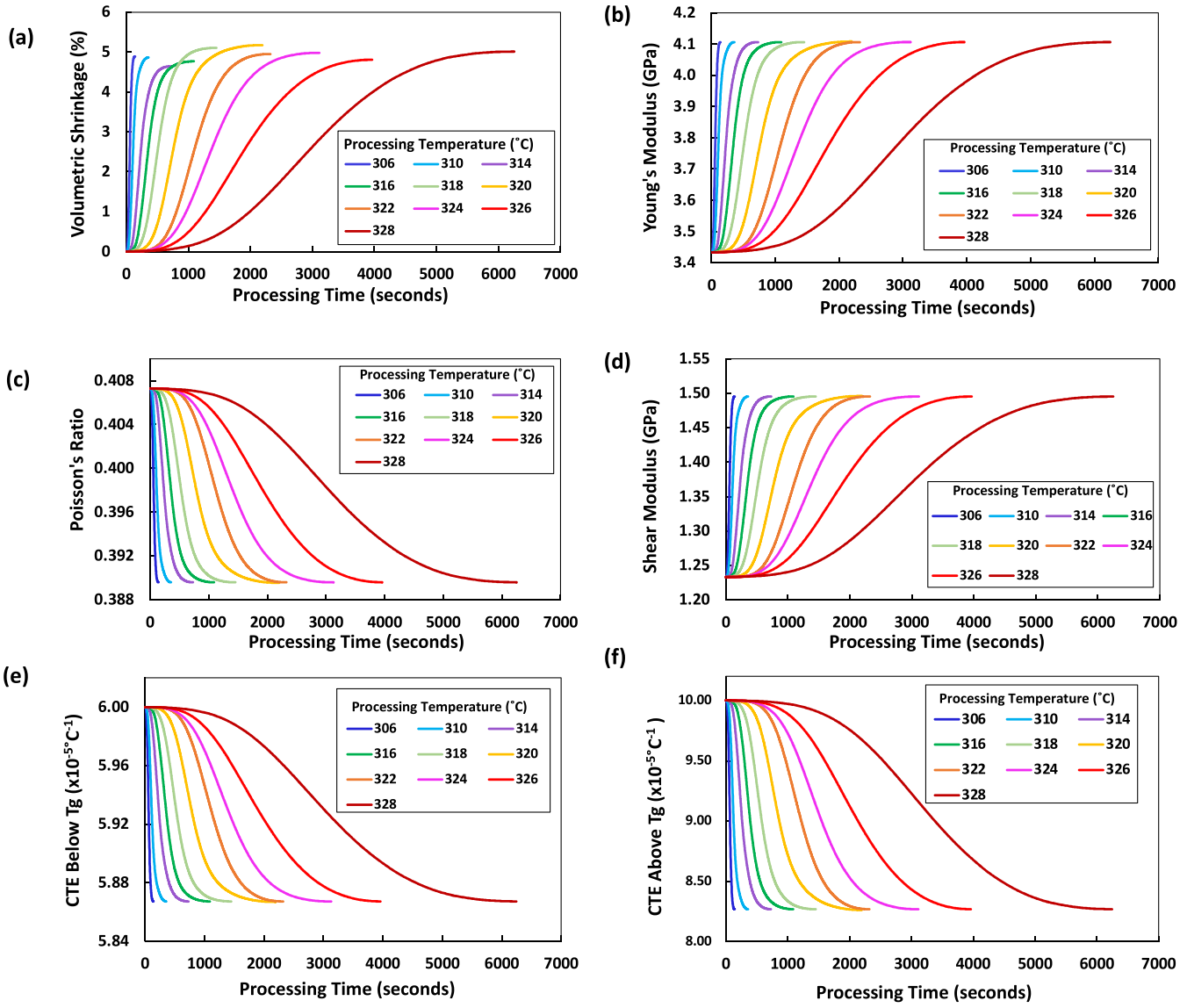

Figure 5. Evolution of (a) volumetric shrinkage, (b) Young's modulus, (c) Poisson's ratio, (d) shear modulus, and (e, f) coefficient of thermal expansion as a function of processing time for varying processing temperatures.

attributable to the faster crystal growth associated with these temperatures (Figure S6).

Figure 5b–d present the change in elastic properties during the processing of semicrystalline PEEK. Similar to the volumetric shrinkage predictions, evolution of mechanical properties during processing highly depends on the processing temperature. As the processing temperature increases, the secondary crystallization mechanism accelerates.[66−68] The secondary crystallization is much slower than the primary crystallization, which explains the longer processing time at higher processing temperatures.

Figure 5e,5f show the evolution of the CTE below and above T_g, respectively, for semicrystalline PEEK. In both cases, the CTE evolves more slowly for higher processing temperatures. Similar to the semicrystalline elastic properties, the slower crystallization rate at the higher processing temperatures slows the evolution of the CTE to its crystalline value.

CONCLUSIONS

Using multiscale process modeling, the results of this study indicate that semicrystalline PEEK thermomechanical properties are highly dependent on the crystallinity content, which is, in turn, dependent on the annealing temperature during processing. Within the annealing temperature range of 306–328 °C, lower temperatures provide higher crystallization rates (rapidly evolving the bulk properties to their crystalline values) and higher temperatures provide slower crystallization rates (slowly evolving the bulk properties to their crystallization rates). Similarly, the volumetric shrinkage increases more rapidly for lower temperatures in the temperature range.

Because volumetric shrinkage is directly responsible for the production of residual stresses in thermoplastic composites, it follows that slower volumetric shrinkage times (corresponding to the lower crystallization rate from higher processing temperatures) will allow the material more time to accommodate the residual stresses through volumetric relaxation before the final cool-down processing cycle. Therefore, higher processing temperatures in the range

https://doi.org/10.1021/acsaenm.3c00586
ACS Appl. Eng. Mater. 2023, 1, 3167−3177

considered in this study (306−328 °C) may be advantageous from this perspective.

The results of this study are important for the future development of next-generation thermoplastic materials and thermoplastic fiber-reinforced composite materials and structures. Although trial-and-error approaches have been used in the past for optimizing processing parameters for new polymer materials, computationally driven approaches based on Materials Genome Initiative (MGI) principles[70] are much more promising for rapid optimization of processing parameters for demanding engineering environments. Moving forward, the protocols outlined in this paper can be used for a newer generation of thermoplastics for rapid process design and technological insertion.

■ ASSOCIATED CONTENT

Supporting Information

The Supporting Information is available free of charge at https://pubs.acs.org/doi/10.1021/acsaenm.3c00586.

PEEK polymerization details, shear stress−strain curves of amorphous PEEK, thermal properties, elastic properties of crystalline PEEK, relative crystallinity, and calculation of elastic constants (PDF)

■ AUTHOR INFORMATION

Corresponding Author

Gregory M. Odegard − *Michigan Technological University, Houghton, Michigan 49931, United States;* orcid.org/0000-0001-7577-6565; Email: gmodegar@mtu.edu

Authors

Khatereh Kashmari − *Michigan Technological University, Houghton, Michigan 49931, United States;* orcid.org/0009-0007-4406-3635

Hashim Al Mahmud − *Faculty of Engineering, University of Kufa, Najaf 54001, Iraq*

Sagar U. Patil − *Michigan Technological University, Houghton, Michigan 49931, United States;* orcid.org/0000-0003-4301-777X

William A. Pisani − *Michigan Technological University, Houghton, Michigan 49931, United States*

Prathamesh Deshpande − *Michigan Technological University, Houghton, Michigan 49931, United States;* orcid.org/0000-0003-1441-678X

Marianna Maiaru − *University of Massachusetts Lowell, Lowell, Massachusetts 01854, United States*

Complete contact information is available at: https://pubs.acs.org/10.1021/acsaenm.3c00586

Notes

The authors declare no competing financial interest.

■ ACKNOWLEDGMENTS

This research was partially supported by the Richard and Elizabeth Henes Endowment at Michigan Technological University, the NASA Space Technology Research Institute (STRI) for Ultra-Strong Composites by Computational Design (US-COMP), grant NNX17AJ32G, and NASA grant 80NSSC19K1246. SUPERIOR, a high-performance computing cluster at Michigan Technological University, was used in obtaining the MD simulation results presented in this study.

■ REFERENCES

(1) Chapman, T. J.; Gillespie, J. W., Jr.; Pipes, R. B.; Manson, J.-A. E.; Seferis, J. C. Prediction of Process-Induced Residual Stresses in Thermoplastic Composites. *J. Compos. Mater.* **1990**, *24* (6), 616−643.

(2) Talbott, M. F.; Springer, G. S.; Berglund, L. A. The Effects of Crystallinity on the Mechanical Properties of PEEK Polymer and Graphite Fiber Reinforced PEEK. *J. Compos. Mater.* **1987**, *21* (11), 1056−1081.

(3) Pisani, W. A.; Radue, M. S.; Chinkanjanarot, S.; Bednarcyk, B. A.; Pineda, E. J.; Waters, K.; Pandey, R.; King, J. A.; Odegard, G. M. Multiscale Modeling of PEEK using Reactive Molecular Dynamics Modeling and Micromechanics. *Polymer* **2019**, *163*, 96−105.

(4) Wang, Y.; Beard, J. D.; Evans, K. E.; Ghita, O. Unusual Crystalline Morphology of Poly Aryl Ether Ketones (PAEKs). *RSC Adv.* **2016**, *6* (4), 3198−3209.

(5) Blundell, D. J.; Willmouth, F. M. Crystalline Morphology of the Matrix of PEEK-Carbon Fiber Aromatic Polymer Composites. *SAMPE Q.* **1986**, *17*, 50−57.

(6) Hudson, S. D.; Davis, D. D.; Lovinger, A. J. Semicrystalline Morphology of Poly (Aryl Ether Ether Ketone)/Poly (Ether imide) Blends. *Macromolecules* **1992**, *25* (6), 1759−1765.

(7) Parlevliet, P. P.; Bersee, H. E.; Beukers, A. Residual Stresses in Thermoplastic Composites—A Ctudy of the Literature—Part I: Formation of Residual Stresses. *Composites, Part A* **2006**, *37* (11), 1847−1857.

(8) Deshpande, P.; Patil, S.; Shah, S.; Kashmari, K.; Olaya, M.; Odegard, G. M.; Maiarã, M. In *A Multi-Scale Approach for Modelling the Cure of Thermoset Polymers within ICME*, Proceedings of the American Society for Composites, Thirty-Fourth Technical Conference, 2019.

(9) Patil, S.; Deshpande, P.; Shah, S.; Kashmari, K.; Odegard, G. M.; Maiaru, M. In *Prediction of Residual Stress Build-Up in Polymer Matrix Composite During Cure Using a Two-Scale Approach*, Proceedings of the American Society for Composites, Thirty-Fourth Technical Conference, 2019.

(10) Li, M. C.; Wu, J. J.; Loos, A. C.; Morton, J. A Plane-strain Finite Element Model for Process-Induced Residual Stresses in a Graphite/PEEK Composite. *J. Compos. Mater.* **1997**, *31* (3), 212−243.

(11) D'Mello, R. J.; Maiaru, M.; Waas, A. M. Virtual Manufacturing of Composite Aerostructures. *Aeronaut. Sci.* **2016**, *120* (1223), 61−81.

(12) D'Mello, R.; Waas, A.; Maiaru, M.; Koon, R. In *Integrated Computational Modeling for Efficient Material and Process Design for Composite Aerospace Structures*, AIAA Scitech 2020 Forum, 2020.

(13) D'Mello, R. J.; Maiarù, M.; Waas, A. M. Effect of the Curing Process on the Transverse Tensile Strength of Fiber-Reinforced Polymer Matrix Lamina Using Micromechanics Computations. *Integr. Mater. Manuf. Innovation* **2015**, *4* (1), 119−136.

(14) MAIARÙ, M.; D'mello, R. J.; Waas, A. M. In *Virtual Testing for the Mechanical Characterization of Cured Polymer Matrix Composites*, Proceedings of the American Society for Composites, Thirty-second Technical Conference, 2017.

(15) Shah, S.; Patil, S.; Deshpande, P.; Krieg, A.; Kashmari, K.; Al Mahmud, H.; King, J.; Odegard, G. M.; Maiaru, M. In *Multiscale Modeling for Virtual Manufacturing of Thermoset Composites*, AIAA Scitech 2020 Forum, 2020.

(16) Maiaru, M. In *Effect of Uncertainty in Matrix Fracture Properties on the Transverse Strength of Fiber Reinforced Polymer Matrix Composites*, AIAA/ASCE/AHS/ASC Structures, Structural Dynamics, and Materials Conference, 2018.

(17) Maiarù, M.; D'Mello, R. J.; Waas, A. M. Characterization of Intralaminar Strengths of Virtually Cured Polymer Matrix Composites. *Composites, Part B* **2018**, *149*, 285−295.

(18) Shah, S.; Maiaru, M. In *Microscale Analysis of Virtually Cured Polymer Matrix Composites Accounting for Uncertainty in Matrix Properties During Manufacturing*, Proceedings of the American Society for Composites, Thirty-Third Technical Conference, 2018.

(19) Shah, S. P.; Patil, S. U.; Hansen, C. J.; Odegard, G. M.; Maiarù, M. Process Modeling and Characterization of Thermoset Composites

for Residual Stress Prediction. *Mech. Adv. Mater. Struct.* **2023**, *30* (3), 486−497.
(20) Patil, S.; Shah, S.; Deshpande, P.; Kashmari, K.; Olaya, M.; Odegard, G. M.; Maiarã, M. In *Multi-Scale Approach to Predict Cure-Induced Residual Stresses in an Epoxy System*, Proceedings of the American Society for Composites, Thirty-Fifth Technical Conference, 2020.
(21) Kashmari, K.; Deshpande, P.; Patil, S.; Shah, S.; Maiaru, M.; Odegard, G. M. In *Prediction of PEEK Resin Properties for Processing Modeling Using Molecular Dynamics*, Proceedings of the American Society for Composites,Thirty-Sixth Technical Conference on Composite Materials, 2021.
(22) Shah, S. P.; Maiarù, M. Effect of Manufacturing on the Transverse Response of Polymer Matrix Composites. *Polymers* **2021**, *13* (15), No. 2491.
(23) Al Mahmud, H.; Radue, M. S.; Pisani, W. A.; Odegard, G. M. Computational Modeling of Hybrid Carbon Fiber/Epoxy Composites Reinforced with Functionalized and Non-Functionalized Graphene Nanoplatelets. *Nanomaterials* **2021**, *11* (11), No. 2919.
(24) Kashmari, K.; Patil, S.; Deshpande, P.; Shah, S.; Maiaru, M.; Odegard, G. M. Molecular Modeling of PEEK Resins for Prediction of Properties in Process Modeling. *Earth Space* **2021**, 104−112.
(25) Seo, J.; Gohn, A. M.; Dubin, O.; Takahashi, H.; Hasegawa, H.; Sato, R.; Rhoades, A. M.; Schaake, R. P.; Colby, R. H. Isothermal Crystallization of Poly (Ether Ether Ketone) with Different Molecular Weights Over a Wide Temperature Range. *Polym. Cryst.* **2019**, *2* (1), No. e10055.
(26) Schuster, M. *Characterization of Laminated Safety Glass Interlayers: Thermorheology, Crystallinity and Viscoelasticity*; Springer Nature, 2022; Vol. *66*.
(27) Velikov, V. H., Jr. Time Dependent Properties of Semicrystalline Poly (Arylene Ether Ether Ketone)(PEEK) Above and Below the Glass Transition. Ph.D. Thesis; Virginia Tech, 1996.
(28) Heinz, H.; Lin, T.-J.; Mishra, R.; Emami, F. S. Thermodynamically Consistent Force Fields for the Assembly of Inorganic, Organic, and Biological Nanostructures: the Interface Force Field. *Langmuir* **2013**, *29* (6), 1754−1765.
(29) Odegard, G. M.; Patil, S. U.; Gaikwad, P. S.; Deshpande, P.; Krieg, A. S.; Shah, S. P.; Reyes, A.; Dickens, T.; King, J. A.; Maiaru, M. Accurate Predictions of Thermoset Resin Glass Transition Temperatures from All-atom Molecular Dynamics Simulation. *Soft Matter* **2022**, *18* (39), 7550−7558.
(30) Patil, S. U.; Shah, S. P.; Olaya, M.; Deshpande, P. P.; Maiaru, M.; Odegard, G. M. Reactive Molecular Dynamics Simulation of Epoxy for the Full Cross-linking Process. *ACS Appl. Polym. Mater.* **2021**, *3* (11), 5788−5797.
(31) Winetrout, J. J.; Kanhaiya, K.; Sachdeva, G.; Pandey, R.; Damirchi, B.; van Duin, A.; Odegard, G.; Heinz, H. Implementing Reactivity in Molecular Dynamics Simulations with the Interface Force Field (IFF-R) and Other Harmonic Force Fields, arXiv:2107.14418v1. arXiv.org e-Print archive, 2021. https://arxiv.org/abs/2107.14418.
(32) Gaikwad, P. S.; Krieg, A. S.; Deshpande, P. P.; Patil, S. U.; King, J. A.; Maiaru, M.; Odegard, G. M. Understanding the Origin of the Low Cure Shrinkage of Polybenzoxazine Resin by Computational Simulation. *ACS Appl. Polym. Mater.* **2021**, *3* (12), 6407−6415.
(33) Pisani, W. A.; Wedgeworth, D. N.; Roth, M. R.; Newman, J. K.; Shukla, M. K. Computational Prediction of Mechanical Properties of PA6−Graphene/Carbon Nanotube Nanocomposites. *J. Phys. Chem. C* **2021**, *125* (28), 15569−15578.
(34) Pisani, W. A.; Newman, J. K.; Shukla, M. K. Multiscale Modeling of Polyamide 6 Using Molecular Dynamics and Micromechanics. *Ind. Eng. Chem. Res.* **2021**, *60* (37), 13604−13613.
(35) Pisani, W. A.; Wedgeworth, D. N.; Roth, M. R.; Newman, J. K.; Shukla, M. K. *Exploration of Two Polymer Nanocomposite Structure-Property Relationships Facilitated by Molecular Dynamics Simulation and Multiscale Modeling*; US Army Engineer Research and Development Center: Vicksburg, Miss, 2023.
(36) Nosé, S. A Molecular-Dynamics Method for Simulations in the Canonical Ensemble. *Mol. Phys.* **1984**, *52* (2), 255−268.
(37) Hoover, W. G. Canonical Dynamics - Equilibrium Phase-Space Distributions. *Phys. Rev. A* **1985**, *31* (3), 1695−1697.
(38) Shanno, D. F. Conjugate Gradient Methods with Inexact Searches. *Math. Oper. Res.* **1978**, *3* (3), 244−256.
(39) Gissinger, J. R.; Jensen, B. D.; Wise, K. E. Modeling Chemical Reactions in Classical Molecular Dynamics Simulations. *Polymer* **2017**, *128*, 211−217.
(40) Blundell, D. J.; Osborn, B. N. The Morphology of Poly (Aryl-Ether-Ether-Ketone). *Polymer* **1983**, *24* (8), 953−958.
(41) Odegard, G. M.; Patil, S. U.; Deshpande, P. P.; Kanhaiya, K.; Winetrout, J. J.; Heinz, H.; Shah, S. P.; Maiaru, M. Molecular Dynamics Modeling of Epoxy Resins Using the Reactive Interface Force Field. *Macromolecules* **2021**, *54* (21), 9815−9824.
(42) Shenogina, N. B.; Tsige, M.; Patnaik, S. S.; Mukhopadhyay, S. M. Molecular modeling of elastic properties of thermosetting polymers using a dynamic deformation approach. *Polymer* **2013**, *54* (13), 3370−3376.
(43) KetaSpire, P. *Design & Processing Guide*. version; Solvay Specialty Polymers, 2013.
(44) Lee, W. I.; Talbott, M. F.; Springer, G.; Berglund, L. A. Effects of Cooling rate on the Crystallinity and Mechanical Properties of Thermoplastic Composites. *J. Reinf. Plast. Compos.* **1987**, *6* (1), 2−12.
(45) Odegard, G. M.; Jensen, B. D.; Gowtham, S.; Wu, J.; He, J.; Zhang, Z. Predicting Mechanical Response of Crosslinked Epoxy using ReaxFF. *Chem. Phys. Lett.* **2014**, *591*, 175−178.
(46) Lee, Y.; Porter, R. S. Crystallization of Poly (etheretherketone)-(PEEK) in Carbon Fiber Composites. *Polym. Eng. Sci.* **1986**, *26* (9), 633−639.
(47) Bandyopadhyay, A.; Valavala, P. K.; Clancy, T. C.; Wise, K. E.; Odegard, G. M. Molecular modeling of crosslinked epoxy polymers: The effect of crosslink density on thermomechanical properties. *Polymer* **2011**, *52* (11), 2445−2452.
(48) Chinkanjanarot, S.; Radue, M. S.; Gowtham, S.; Tomasi, J. M.; Klimek-McDonald, D. R.; King, J. A.; Odegard, G. M. Multiscale Thermal Modeling of Cured Cycloaliphatic Epoxy/Carbon Fiber Composites. *J. Appl. Polym. Sci.* **2018**, *135* (25), No. 46371.
(49) Radue, M. S.; Varshney, V.; Baur, J. W.; Roy, A. K.; Odegard, G. M. Molecular Modeling of Cross-Linked Polymers with Complex Cure Pathways: A Case Study of Bismaleimide Resins. *Macromolecules* **2018**, *51* (5), 1830−1840.
(50) Odegard, G. M.; Bandyopadhyay, A. Physical Aging of Epoxy Polymers and Their Composites. *J. Polym. Sci., Part B: Polym. Phys.* **2011**, *49* (24), 1695−1716.
(51) Toft, M. The Effect of Crystalline Morphology on the Glass Transition and Enthalpic Relaxation in Poly (Ether-Ether-Ketone). Ph.D. Thesis; University of Birmingham, 2012.
(52) Choy, C. L.; Leung, W. P.; Nakafuku, C. Thermal Expansion of Poly (Ether-Ether-Ketone)(PEEK). *J. Polym. Sci., Part B: Polym. Phys.* **1990**, *28* (11), 1965−1977.
(53) King, M. A.; Blundell, D.; Howard, J.; Colbourn, E.; Kendrick, J. Modelling studies of crystalline PEEK. *Mol. Simul.* **1989**, *4* (1−3), 3−13.
(54) Patil, S. U.; Krieg, A. S.; Odegard, L. K.; Yadav, U.; King, J. A.; Maiaru, M.; Odegard, G. M. Simple and convenient mapping of molecular dynamics mechanical property predictions of bisphenol-F epoxy for strain rate, temperature, and degree of cure. *Soft Matter* **2023**, *19* (35), 6731−6742.
(55) Chen, F.; Ou, H.; Lu, B.; Long, H. A Constitutive Model of Polyether-Ether-Ketone (PEEK). *J. Mech. Behav. Biomed. Mater.* **2016**, *53*, 427−433.
(56) Rae, P. J.; Brown, E. N.; Orler, E. B. The Mechanical Properties of Poly (Ether-Ether-Ketone)(PEEK) with Emphasis on the Large Compressive Strain Response. *Polymer* **2007**, *48* (2), 598−615.
(57) Aboudi, J.; Arnold, S. M.; Bednarcyk, B. A. *Micromechanics of Composite Materials: A Generalized Multiscale Analysis Approach*; Butterworth-Heinemann, 2013.

https://doi.org/10.1021/acsaenm.3c00586
ACS Appl. Eng. Mater. 2023, 1, 3167−3177

(58) Fischer, C.; Drummer, D. Crystallization and Mechanical Properties of Polypropylene under Processing-Relevant Cooling Conditions with Respect to Isothermal Holding Time. *Int. J. Polym. Sci.* **2016**, *2016*, No. 5450708, DOI: 10.1155/2016/5450708.
(59) Corrigan, E.; Leach, D.; McDaniels, T. *The Influence of Processing Conditions on the Properties of PEEK Matrix Composites, in Materials and Processing-Move into the 90′s*; Benson, S.et al., Ed.; Elsevier: Amsterdam, 1989; pp 121−131.
(60) Sonmez, F. O.; Hahn, H. T. In *Simulation of Crystallization Behavior During Thermoplastic Tape Placement Process*, Proceedings of the Tenth International Conference on Composite Materials (ICCM): Whistler, Canada, 1995.
(61) Motz, H.; Schultz, J. M. The Solidification of PEEK. Part I: Morphology. *J. Thermoplast. Compos. Mater.* **1989**, *2* (4), 248−266.
(62) Motz, H.; Schultz, J. M. The Solidification of PEEK. Part II: Kinetics. *J. Thermoplast. Compos. Mater.* **1989**, *2* (4), 267−280.
(63) Harris, L. A Study of the Crystallisation Kinetics in PEEK and PEEK Composites. Ph.D. Thesis; University of Birmingham, 2011.
(64) Cowie, J. M. G.; Arrighi, V. *Polymers: Chemistry and Physics of Modern Materials*; CRC Press, 2007.
(65) Tardif, X.; Pignon, B.; Boyard, N.; Schmelzer, J. W.; Sobotka, V.; Delaunay, D.; Schick, C. Experimental Study of Crystallization of PolyEtherEtherKetone (PEEK) Over a Large Temperature Range Using a Nano-calorimeter. *Polym. Test.* **2014**, *36*, 10−19.
(66) Bessard, E.; De Almeida, O.; Bernhart, G. Unified isothermal and non-isothermal modelling of neat PEEK crystallization. *J. Therm. Anal. Calorim.* **2014**, *115* (2), 1669−1678.
(67) Velisaris, C. N.; Seferis, J. C. Crystallization Kinetics of Polyetheretherketone (PEEK) Matrices. *Polym. Eng. Sci.* **1986**, *26* (22), 1574−1581.
(68) Cebe, P. Application of the Parallel Avrami Model to Crystallization of Poly (etheretherketone). *Polym. Eng. Sci.* **1988**, *28* (18), 1192−1197.
(69) Ko, T. Y.; Woo, E. M. Changes and Distribution of Lamellae in the Spherulites of Poly (Ether Ether Ketone) upon Stepwise Crystallization. *Polymer* **1996**, *37* (7), 1167−1175.
(70) Odegard, G. M.; Liang, Z.; Siochi, E. J.; Warren, J. A. A successful strategy for MGI-inspired research. *MRS Bull.* **2023**, *48*, 434−438.

https://doi.org/10.1021/acsaenm.3c00586
ACS Appl. Eng. Mater. 2023, 1, 3167−3177